J Solid State Electrochem (2017) 21:1297–1303
DOI 10.1007/s10008-016-3470-6

ORIGINAL PAPER

Ethylenediamine tetramethylene phosphonic acid assisted synthesis of palladium nanocubes and their electrocatalysis of formic acid oxidation

Ruopeng Zhao[1,2,3] · **Zhenyuan Liu**[2] · **Mingxing Gong**[2] · **Qingwen Zhang**[1,3] · **Xinhao Shi**[1,3] · **Yongqi Hu**[1,3] · **Weiye Qi**[1,3] · **Yawen Tang**[2] · **Yi Wang**[1,3]

Received: 9 June 2016 / Revised: 7 November 2016 / Accepted: 10 November 2016 / Published online: 9 December 2016

Abstract The synthesis of Pd nanocrystals of controlled size and morphology has drawn enormous interest due to their catalytic activity. We report a new and efficient strategy for the one-step synthesis of monodispersed Pd nanocubes with ethylenediamine tetramethylene phosphonate (EDTMP) as a complex-forming and capping agent. The morphology, structure, and growth mechanism of the Pd nanocubes were fully characterized via selected area electron diffraction (SAED), transmission electron microscopy (TEM), X-ray diffraction (XRD), and X-ray photoelectron spectroscopy (XPS). It was found that the morphology of the Pd nanocrystals in the proposed EDTMP–$PdCl_2$ system could be changed from octahedrons to nanocubes simply by adjusting the amount of iodide used during synthesis. After UV/ozone and electrochemical cleaning, the as-prepared Pd nanocubes demonstrated excellent electrocatalytic activity and stability during formic acid oxidation, owing to their abundant {100} facets and small particle size.

Electronic supplementary material The online version of this article (doi:10.1007/s10008-016-3470-6) contains supplementary material, which is available to authorized users.

✉ Yawen Tang
tangyawen@njnu.edu.cn

✉ Yi Wang
wangyi@wibe.ac.cn

[1] Institute of Biomaterials and Engineering, Wenzhou Medical University, Wenzhou 325000, China

[2] Jiangsu Key Laboratory of New Power Batteries, Jiangsu Collaborative Innovation Center of Biomedical Functional Materials, School of Chemistry and Materials Science, Nanjing Normal University, Nanjing 210023, China

[3] Wenzhou Institute of Biomaterials and Engineering, Chinese Academy of Sciences, Wenzhou 325000, China

Keywords One-step · Palladium · Nanocube · Ethylenediamine tetramethylene phosphonic acid · Formic acid oxidation reaction

Introduction

The shape of a noble metal nanocrystal plays a significant role in its catalytic activity and selectivity, as it influences the distribution of surface atoms at corners, edges, and planes. Thus, the synthesis of metal nanocrystals with various morphologies has received a great deal of interest in recent years [1–12].

Pd nanocrystals are among the most studied of the noble metal nanocrystals. Pd nanocrystals with diverse morphologies have been synthesized, including wires [13], spheres [14], tubes [15], cubes [16], plates [17], rods [18–20], tetrahexahedra [21], cubooctahedra [22], octahedra [23], tetrahedra [24], and concave tetrahedra [25]. Among various shapes, {100}-enclosed Pd nanocubes are of particular interest in relation to formic acid oxidation because the {100} facet of Pd shows the highest catalytic activity among the three low-index facets (Pd{100} > Pd{111} > Pd{110}) [26]. Therefore, these {100}-enclosed Pd nanocubes appear to be particularly useful for direct formic acid fuel cell (DFAFC) applications.

More recently, the specific adsorption of small molecules on Pd or Pd-based nanocrystal surfaces has emerged as a promising strategy for controlling surface structure [19, 27, 28]. For instance, Zheng and coworkers reported that CO prefers to adsorb on the Pd {111} surface, and that this adsorption of CO facilitates the growth of single-crystalline Pd tetrapods with {111} facets as their main exposed surfaces [29]. However, there are hidden dangers such as CO leakage during the preparation process. Xia and coworkers demonstrated that the adsorption of bromide ions on the Pd {100} surface makes

the Pd {100} facet more energetically stable than Pd {111} and results in the formation of Pd nanocubes [30], although the two-step preparation process was somewhat complicated. Maiyalagan and coworkers explored a novel method allowing the synthesis of tailored Pd nanostructures. The products showed anisotropic nanostructure consisting of chains of cubes which presented superior electrocatalytic activity. However, the Pd cubes were not uniform in size [31].

Herein, we report a simple and efficient strategy for the one-step synthesis of Pd nanocubes with the assistance of ethylenediamine tetramethylene phosphonic acid (EDTMP) and I^-. In the reaction system, I^- serves as a shape control agent, EDTMP works as a chelating agent, HCHO acts as a reductant, and PVP acts as a stabilizing agent. The resulting Pd nanocubes exhibit enhanced electrocatalytic activity and stability during formic acid oxidation compared to the commercially used catalyst Pd black, owing to their abundant exposed {100} facets and small particle size.

Experimental section

Reagents and chemicals

Palladium chloride ($PdCl_2$), formaldehyde solution (HCHO, 40 %), and polyvinylpyrrolidone (PVP) were purchased from Sinopharm Chemical Reagent Co., Ltd. (Shanghai, China). Ethylenediamine tetramethylene phosphonic acid (EDTMP) was purchased from Shandong Taihe Water Treatment Co., Ltd. (Shandong, China). KI was purchased from Aladdin Industrial Corporation (Shanghai, China). Commercial Pd black was purchased from Johnson Matthey Corporation (London, UK). Other reagents were analytical reagent grade and used without further purification. All the aqueous solutions were prepared with Millipore (Billerica, MA, USA) water with a resistivity of 18.2 MΩ. Solution pH was adjusted through the addition of dilute NaOH or HCl solution.

Preparation of the Pd nanocubes

In a typical synthesis, 1 mL of 0.05 M $PdCl_2$, 1 mL of 0.05 M EDTMP, 0.01 g KI, and 0.01 g PVP were added to 7 mL deionized water with continuous stirring. After adjusting the solution pH to 7.0, 0.5 mL of an HCHO solution (40 %) was added to the solution. Then, the mixture was transferred to a 25-mL Teflon-lined stainless-steel autoclave and heated at 140 °C for 6 h. After being cooled to room temperature, the resulting Pd nanocubes were separated by centrifugation at 19,000 rpm for 10 min, washed several times with water and ethanol, and then dried at 60 °C for 5 h in a vacuum dryer.

Physical characterization

Transmission electron microscope (TEM) measurements were performed on a JEOL (Tokyo, Japan) JEM-2100 F transmission electron microscope operated at an accelerating voltage of 200 kV. Scanning electron microscopy (SEM) images were captured on a JSM-2010 microscope (JEOL) at an accelerating voltage of 20 kV. X-ray diffraction (XRD) patterns of nanocrystals were obtained using a D/max-rC X-ray diffractometer (Rigaku, Tokyo, Japan) with a CuKα radiation source ($\lambda = 1.5406$ Å) and operating at 40 kV and 100 mA. X-ray photoelectron spectroscopy (XPS) measurements were performed with a Thermo Scientific (Waltham, MA, USA) ESCALAB 250 spectrometer with a monochromatic Al Ka X-ray source (1486.6-eV photons), and the vacuum in the analysis chamber was maintained at about 10^{-9} mbar. The binding energy was calibrated by means of the C_{1s} peak energy of 284.6 eV. The pH measurements were carried out with a Mettler Toledo (Columbus, OH, USA) DETTA320 digital pH-meter.

Electrochemical measurements

All electrochemical experiments were performed using a CHI 660 C electrochemical analyzer (CH Instruments, Austin, TX, USA). A standard three-electrode system was used for all electrochemical experiments, which consisted of a Pt wire as

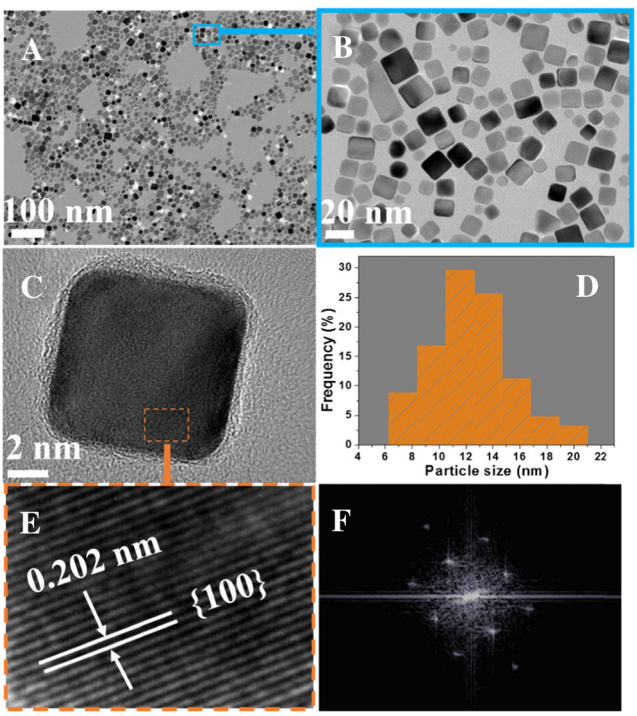

Fig. 1 **a** Typical and **b** magnified TEM images of Pd nanocubes. **c** HRTEM image of an individual Pd nanocube. **d** The size distribution histogram for the Pd nanocubes shown in **a**. **e** Magnified HRTEM images obtained from regions marked by *squares* in **c.** **f** FFT pattern for **e**

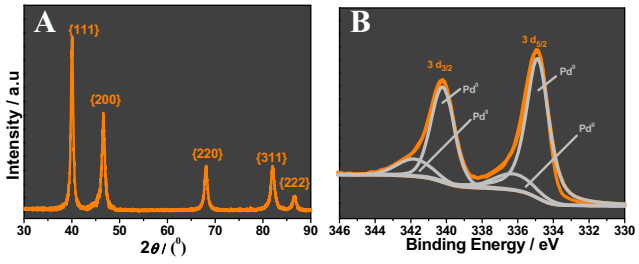

Fig. 2 **a** XRD pattern of Pd nanocubes. **b** XPS spectrum of Pd nanocubes in the Pd 3*d* region

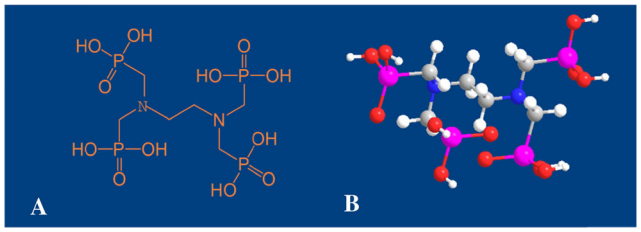

Scheme 1 **a** Molecular structure and **b** cylindrical bond model of EDTMP

the auxiliary electrode, a saturated calomel reference electrode (SCE), and a catalyst-modified glassy carbon electrode as the working electrode. In this study, all stated potentials are given with respect to the SCE. All electrochemical measurements were carried out at 30 °C.

Before the preparation of the catalyst ink, the Pd nanocubes were irradiated with UV irradiation (185 and 254 nm) in air for 4 h to remove the capping agents (i.e., PVP and I^-) [32–36]. Note that an irradiation time of less than 5 h was used to avoid particle coalescence during long periods of irradiation (see the TEM and XRD results for the Pd nanocubes before and after UV irradiation in Fig. S1 of the "Electronic supplementary material," ESM). An evenly distributed suspension of the catalyst was prepared by ultrasonication of a mixture comprising a certain amount of catalyst in an appropriate amount of water for 30 min. Then, a predetermined amount of the dispersion was drop cast onto the surface of a pretreated glassy carbon electrode. After drying at room temperature, the modified electrode surface was covered with 2 mL of Nafion solution (5 wt.%) and allowed to dry again. Thus, the working electrode was obtained, and the specific loading of metal on the electrode surface was about 3.5 μg. Prior to performing electrochemical tests, the catalyst-coated electrodes were pretreated by cycling the potential between −0.2 and 1.2 V vs. SCE for 50 cycles to remove any possible contaminants on the Pd. Cyclic voltammetry measurements were conducted in N_2-saturated 0.05 M H_2SO_4 solution or N_2-saturated 0.5 M H_2SO_4 solution with 0.5 M HCOOH. The electrochemically active surface area (ESCA) of the Pd electrocatalyst was calculated using the following equation by measuring the reduction charge of the $Pd(OH)_2$ on the surface and assuming a value of 420 μC cm^{-2} for the reduction charge of a monolayer of $Pd(OH)_2$ on a Pd surface [37, 38]:

$$\mathrm{ECSA} = \frac{Q}{m \times C} \quad (1)$$

where Q is the reduction charge of the surface $Pd(OH)_2$, m is the amount of Pd metal loaded, and C is the charge required for the adsorption of a monolayer of hydrogen on a Pd surface ($C = 420$ μC cm^{-2}).

Results and discussion

The structure and morphology of the Pd nanocrystals were first characterized using transmission electron microscopy (TEM) and scanning electron microscopy (SEM). As shown in Fig. 1a, b and Fig. S2 of the ESM, the as-prepared Pd nanocrystals were well-defined cubes. According to the histogram showing the particle size distribution of the as-prepared Pd nanocubes, the average length of a Pd nanocube was estimated to be 11 nm. More detailed structural information was provided by high-resolution transmission electron microscopy (HRTEM). Fringes with a lattice spacing of 0.202 nm (Fig. 1e and Fig. S3 in the ESM) were observed on the surface of the cube, similar to the {100} lattice spacing of the fcc Pd crystal (0.200 nm). The corresponding fast Fourier transform (FFT)

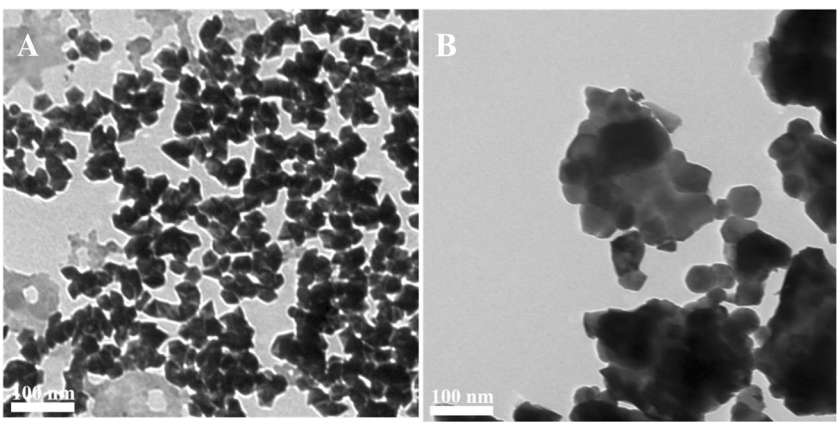

Fig. 3a–b TEM images of the products prepared in the absence of **a** EDTMP or **b** PVP

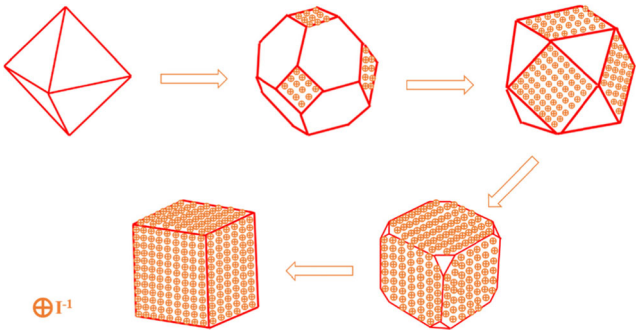

Scheme 2 Schematic illustration of iodide ion adsorption on Pd {100} surfaces, along with the growth of Pd nanocubes

pattern indicates the single-crystalline nature of the Pd cube (Fig. 1f).

The structure of the Pd nanocubes was then investigated by XRD. The Pd nanocubes were observed to have five peaks corresponding to the {111}, {200}, {220}, {311}, and {222} facets of fcc Pd (JCPDS no. 46–1043), respectively (Fig. 2a). Interestingly, the intensity ratio of the {200} peak to the {111} peak for the Pd nanocubes was about 0.75, which is much higher than that of commercial Pd black (0.46, Fig. S4 in ESM) and that of standard Pd according to JCPDS data (0.43), confirming that the products have a {100}-dominated crystalline structure. Among the low-index facets, the Pd {100} facet has the highest catalytic activity (Pd {100} > Pd {111} > Pd {110}) because of its high surface energy [26], which may lead to enhanced catalytic activity during formic acid oxidation. XPS measurements demonstrated that the binding energies of Pd $3d_{3/2}$ and Pd $3d_{5/2}$ are 340.20 and 334.85 eV (Fig. 2b), respectively, using $C_{1s} = 284.6$ eV as a reference, meaning that the interval between them was 5.35 eV. These values are comparable with the standard values for bulk Pd ($3d_{3/2} = 340.15$ eV and $3d_{5/2} = 334.90$ eV). Meanwhile, the percentage of Pd^0 in the Pd nanocubes is ca. 87.3 %, indicating that Pd^{II} species were successfully reduced to metallic Pd.

In order to elucidate the formation mechanism of Pd nanocubes, a series of controlled experiments were conducted. The effect of EDTMP on the morphology of the product was investigated first. When EDTMP was not added, the products obtained consisted mainly of irregular nanoparticles (Fig. 3a). It is well known that a slow reduction rate of the metal precursor is crucial to the generation of high-quality nanocrystals. EDTMP (Scheme 1), a chelating agent, can interact with $PdCl_2$ to form a six-coordinate EDTMP–Pd^{II} complex due to its strong coordinating capability, which significantly decreases the reduction rate of a Pd^{II} precursor [18]. Thus, we predicted that EDTMP would be an excellent kinetic modifier. In the absence of PVP, the final products were dominated by palladium nanoparticle aggregates (Fig. 3b), indicating that PVP acts as a stabilizing agent.

Furthermore, we wanted to determine the role of the iodide ions. Previous reports have noted that Pd nanocrystals enclosed by {100} facets, such as nanocubes and nanobars, can be controlled by Br^- ions. In particular, Xia and his coworkers proposed a reasonable explanation for the influence of the bromide ions on the shape of Pd nanocrystals [30], and we suspect that I^- ions have a similar effect on shape-controlled synthesis. As illustrated in Scheme 2, increasing the amount of I^- causes more and more {100} facets to be exposed. Correspondingly, the morphology of the Pd nanocrystals changed from octahedrons to nanocubes.

To validate this mechanism, the synthesis of Pd nanocrystals with different amounts of iodide ions was carried out. For instance, a synthesis conducted without I^- resulted in Pd octahedrons with a mean size of 12 nm (Fig. 4a). The addition of 30 μM I^- during the synthesis led to truncated nanocubes because the exposed Pd {100} surfaces were stabilized by the relatively scarce I^- ions (Fig. 4b). When the concentration of I^- was increased to 60 μM, regular Pd nanocubes were obtained (Fig. 4c). These results confirmed that the formation of Pd nanocubes can be controlled by adjusting the amount of I^- present during synthesis.

The Pd nanocubes were tested for their electrocatalytic activity during formic acid oxidation. The electrocatalytic activity of the Pd nanocubes was compared with that of commercial Pd black at the same Pd loading. Figure 5a shows cyclic voltammogram (CV) curves of the Pd nanocubes and commercial Pd black recorded in N_2-purged 0.5 M H_2SO_4 solution. Upon measuring the reduction charge of the surface $Pd(OH)_2$, the electrochemically active surface area (ESCA) of the Pd nanocubes (10 $m^2\ g^{-1}$) was found to be higher than

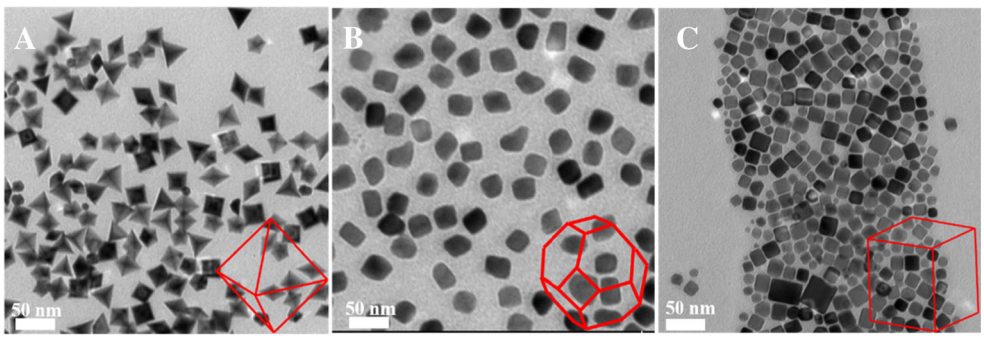

Fig. 4a–c TEM images of Pd nanocrystals synthesized with different amounts of I^- ions: **a** without I^-, **b** 30 μM I^-, **c** 60 μM I^-. An evolution of Pd nanocrystal shape was clearly observed with increasing I^-, from **a** octahedrons to **b** truncated cubes to **c** cubes

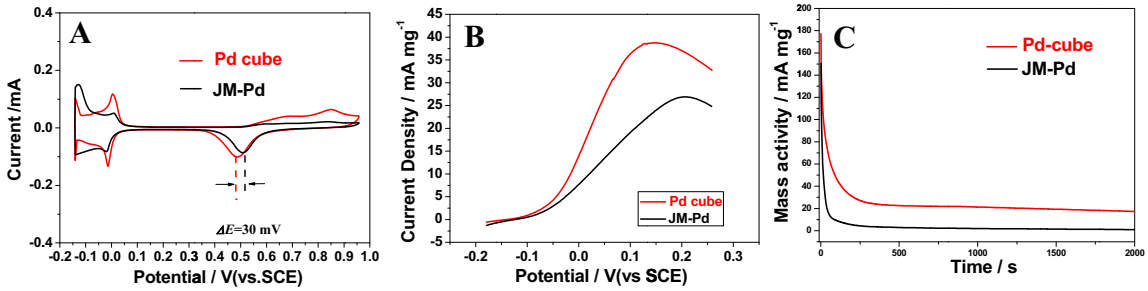

Fig. 5 **a** Cyclic voltammograms of Pd nanocubes and commercial Pd black in N_2-saturated 0.5 M H_2SO_4 solution, sweep rate 50 mVs^{-1}. **b** Quasi-steady-state polarization curves of Pd cubes (*red curve*) and commercial Pd black (*black curve*) measured in 0.5 M HCOOH + 0.5 M H_2SO_4 solution. Scan rate:1 mV s^{-1}. **c** Chronoamperometry curves of Pd nanocubes and commercial Pd black in 0.5 M HCOOH + 0.5 M H_2SO_4 solution for 2000 s at 0.1 V (vs. SCE)

that of commercial Pd black (8 m^2 g^{-1}). This enhanced ESCA for the Pd nanocubes is most likely due to the smaller size and better dispersion of the Pd nanocubes compared with that of commercial Pd black. Furthermore, the reduction peak potential of the Pd nanocubes is negatively shifted by ca. 30 mV compared to that of commercial Pd black, indicating that Pd nanocubes can form more –OH species at a lower potential.

Again, the quasi-steady-state polarization curves obtained at a slow scan rate of 1 mv s^{-1} that are shown in Fig. 5b indicate that the peak potential of the Pd cubes was more negative than that of commercial Pd black, and the Pd cubes exhibited a current density 1.5 times higher than that of commercial Pd black. Both of these observations suggest that the Pd cubes are more electrocatalytically active. Figure S6 in the ESM displays Tafel plots (constructed from the quasi-steady-state data in Fig. 5b) of log *I* vs. *E* for formic acid oxidation at the Pd nanocubes and commercial Pd black in the electrochemical control region. In the lower output current region, both curves remain consistent with a linear Tafel relationship. Under the same output voltage, the Pd nanocubes showed greater output current than commercial Pd black. These results show that the kinetic rate of formic acid oxidation at the Pd nanocubes was higher. Furthermore, the corresponding mass-normalized anodic peak current at the Pd nanocubes was measured as ca. 336 A g^{-1}, which was 1.9 and 1.8 times higher than those of commercial Pd black (175 A g^{-1}, Fig. S7A in the ESM) and commercial Pd/C (185 A g^{-1}, Fig. S5 in the ESM), respectively. Even though its mass activity was lower than that reported by Maiyalagan's group [39], it was better than most of the corresponding values reported in the literature [40, 41]. As shown in Fig. S7B of the ESM, the ESCA-normalized specific peak current density of the Pd-THBTs (27 A m^{-2}) was also higher than that of the commercial Pd black (14 A m^{-2}). The enhanced electrocatalytic activity of the Pd nanocubes was also confirmed by a turnover frequency (TOF, defined here as the HCOOH conversion per surface Pd atom per second) analysis based on the specific activity. The TOF of the Pd nanocubes (2.3 $atom^{-1}s^{-1}$) was found to be 1.5 times higher than that of Pd black (1.5 $atom^{-1}s^{-1}$) at 0.1 V (Fig. S7C in the ESM). Last but not least, the Pd nanocubes showed the improved stability in the DFAFC applications, as indicated by chronoamperometry curves covering a period of 2000 s (Fig. 5c).

Conclusion

In summary, we provide a new one-pot method for the synthesis of Pd nanocubes. During the synthesis of the nanocubes, the presence of EDTMP and I^- were found to be crucial influences on the shape/surface structure of the Pd nanocrystals. EDTMP, an excellent kinetic modifier, induced the formation of high-quality nanocrystals. I^-, a crystal-face-controlling reagent, exerted strong effects on the morphology of the final product. Additionally, the Pd nanocubes exhibited enhanced mass activity, specific activity, and stability during formic acid oxidation compared with commercial Pd black, due to their abundant {100} facets and small particle size. The enhanced properties of the Pb nanocubes facilitate their potential application in direct formic acid fuel cells.

Acknowledgments This research was sponsored by the Wenzhou government's startup fund (WIBEZD2014004-02), the National Natural Science Foundation of China (21376122, 21273116, 21576139, 21503111, and 201605116), the United Fund of NSFC and Yunnan Province (U1137602), and the Industry-Academia Cooperation Innovation Fund Project of Jiangsu Province (BY2012001), a project funded by the Priority Academic Program Development of Jiangsu Higher Education Institutions and the National and Local Joint Engineering Research Center of Biomedical Functional Materials.

References

1. Oh A, Baik H, Choi DS, Cheon JY, Kim B, Kim H, Kwon SJ, Joo SH, Jung Y, Lee K (2015) Skeletal octahedral nanoframe with cartesian coordinates via geometrically precise nanoscale phase segregation in a Pt@ Ni core–shell nanocrystal. ACS Nano 9(3):2856–2867
2. Gong J, Zhou F, Li Z, Tang Z (2013) Controlled synthesis of non-epitaxially grown Pd@ Ag core–shell nanocrystals of interesting optical performance. Chem Commun 49:4379–4381

3. Zhang L, Niu W, Li Z, Xu G (2011) Facile synthesis and electrochemiluminescence application of concave trisoctahedral Pd@ Au core–shell nanocrystals bound by {331} high-index facets. Chem Commun 47:10353–10355
4. Chiu C-Y, Yang M-Y, Lin F-C, Huang J-S, Huang MH (2014) Facile synthesis of Au–Pd core–shell nanocrystals with systematic shape evolution and tunable size for plasmonic property examination. Nanoscale 6:7656–7665
5. Lu N, Wang J, Xie S, Brink J, McIlwrath K, Xia Y, Kim MJ (2014) Aberration corrected electron microscopy study of bimetallic Pd–Pt nanocrystal: core–shell cubic and core–frame concave structures. J Phys Chem C 118:28876–28882
6. Gong K, Park J, Su D, Adzic RR (2014) Metalizing carbon nanotubes with Pd–Pt core–shell nanowires enhances electrocatalytic activity and stability in the oxygen reduction reaction. J Solid State Electrochem 18:1171–1179
7. Chai J, Li F, Bao Y, Liu S, Zhang Q, Niu L (2012) Electrochemical fabrication of multiplicate palladium hierarchical architectures and their electrocatalysis toward oxidation of formic acid. J Solid State Electrochem 16:1203–1210
8. Erikson H, Lüsi M, Sarapuu A, Tammeveski K, Solla-Gullón J, Feliu JM (2016) Oxygen electroreduction on carbon-supported Pd nanocubes in acid solutions. Electrochim Acta 188:301–308
9. Jukk K, Kongi N, Tammeveski K, Solla-Gullón J, Feliu JM (2015) PdPt alloy nanocubes as electrocatalysts for oxygen reduction reaction in acid media. Electrochem Commun 56:11–15
10. Arán-Ais RM, Vidal-Iglesias FJ, Solla-Gull J, Herrero E, Feliu JM (2015) Electrochemical characterization of clean shape-controlled Pt nanoparticles prepared in presence of oleylamine/oleic acid. Electroanalysis 27:945–956
11. Vidal-Iglesias FJ, López-Cudero A, Solla-Gullón J, Aldaz A, Feliu JM (2012) Pd-modified shape-controlled Pt nanoparticles towards formic acid electrooxidation. Electrocatalysis 3:313–323
12. Vidaliglesias FJ, Aránais RM, Sollagullón J, Garnier E, Herrero E, Aldaz A, Feliu JM (2012) Shape-dependent electrocatalysis: formic acid electrooxidation on cubic Pd nanoparticles. Phys Chem Chem Phys 14:10258–10265
13. Campbell MG, Zheng S-L, Ritter T (2013) One-dimensional palladium wires: influence of molecular changes on supramolecular structure. Inorg Chem 52:13295–13297
14. Kim S-W, Kim M, Lee WY, Hyeon T (2002) Fabrication of hollow palladium spheres and their successful application to the recyclable heterogeneous catalyst for Suzuki coupling reactions. J Am Chem Soc 124:7642–7643
15. Cui C-H, Li H-H, Yu S-H (2010) A general approach to electrochemical deposition of high quality free-standing noble metal (Pd, Pt, Au, Ag) sub-micron tubes composed of nanoparticles in polar aprotic solvent. Chem Commun 46:940–942
16. Liu M, Zheng Y, Zhang L, Guo L, Xia Y (2013) Transformation of Pd nanocubes into octahedra with controlled sizes by maneuvering the rates of etching and regrowth. J Am Chem Soc 135:11752–11755
17. Kawasaki A, Itoh S, Shima K, Yamazaki T (2012) Deformation of palladium plates by a small external stress during hydrogen absorption and desorption. Mater Sci Eng A 551:231–235
18. Zhao R, Fu G, Zhou T, Chen Y, Zhu X, Tang Y, Lu T (2014) Multigeneration overgrowth induced synthesis of three-dimensional highly branched palladium tetrapods and their electrocatalytic activity for formic acid oxidation. Nanoscale 6:2776–2781
19. Fu G, Jiang X, Ding L, Tao L, Chen Y, Tang Y, Zhou Y, Wei S, Lin J, Lu T (2013) Green synthesis and catalytic properties of polyallylamine functionalized tetrahedral palladium nanocrystals. Appl Catal B Environ 138:167–174
20. DeSantis CJ, Skrabalak SE (2012) Size-controlled synthesis of Au/Pd octopods with high refractive index sensitivity. Langmuir 28:9055–9062
21. Tian N, Zhou Z-Y, Yu N-F, Wang L-Y, Sun S-G (2010) Direct electrodeposition of tetrahexahedral Pd nanocrystals with high-index facets and high catalytic activity for ethanol electrooxidation. J Am Chem Soc 132:7580–7581
22. Veisz B, Király Z (2003) Size-selective synthesis of cubooctahedral palladium particles mediated by metallomicelles. Langmuir 19:4817–4824
23. Lim B, Xiong Y, Xia Y (2007) A water-based synthesis of octahedral, decahedral, and icosahedral Pd nanocrystals. Angew Chem Int Ed 119:9439–9442
24. Norimatsu FY, Mizokoshi Y, Mori K, Mizugaki T, Ebitani K, Kaneda K (2006) Shape-and size-controlled synthesis of tetrahedral Pd nanoparticles using tetranuclear Pd cluster as precursor. Chem Lett 35:276–277
25. Huang X, Tang S, Zhang H, Zhou Z, Zheng N (2009) Controlled formation of concave tetrahedral/trigonal bipyramidal palladium nanocrystals. J Am Chem Soc 131:13916–13917
26. Lee C-L, Chiou H-P (2012) Methanol-tolerant Pd nanocubes for catalyzing oxygen reduction reaction in H_2SO_4 electrolyte. Appl Catal B Environ 117:204–211
27. Fu G, Tao L, Zhang M, Chen Y, Tang Y, Lin J, Lu T (2013) One-pot, water-based and high-yield synthesis of tetrahedral palladium nanocrystal decorated graphene. Nanoscale 5:8007–8014
28. Fu G, Ding L, Chen Y, Lin J, Tang Y, Lu T (2014) Facile water-based synthesis and catalytic properties of platinum–gold alloy nanocubes. CrystEngComm 16:1606–1610
29. Dai Y, Mu X, Tan Y, Lin K, Yang Z, Zheng N, Fu G (2012) Carbon monoxide-assisted synthesis of single-crystalline Pd tetrapod nanocrystals through hydride formation. J Am Chem Soc 134:7073–7080
30. Peng H-C, Xie S, Park J, Xia X, Xia Y (2013) Quantitative analysis of the coverage density of Br^- ions on Pd {100} facets and its role in controlling the shape of Pd nanocrystals. J Am Chem Soc 135:3780–3783
31. Kannan P, Maiyalagan T, Opallo M (2013) One-pot synthesis of chain-like palladium nanocubes and their enhanced electrocatalytic activity for fuel-cell applications. Nano Energy 2:677–687
32. Zhang Z-C, Hui J-F, Guo Z-G, Yu Q-Y, Xu B, Zhang X, Liu Z-C, Xu C-M, Gao J-S, Wang X (2012) Solvothermal synthesis of Pt–Pd alloys with selective shapes and their enhanced electrocatalytic activities. Nanoscale 4:2633–2639
33. Wang C, Daimon H, Lee Y, Kim J, Sun S (2007) Synthesis of monodisperse Pt nanocubes and their enhanced catalysis for oxygen reduction. J Am Chem Soc 129:6974–6975
34. Yin AX, Min XQ, Zhu W, Liu WC, Zhang YW, Yan CH (2012) Pt-Cu and Pt-Pd-Cu concave nanocubes with high-index facets and superior electrocatalytic activity. Chem Eur J 18:777–782
35. Yin A-X, Min X-Q, Zhu W, Wu H-S, Zhang Y-W, Yan C-H (2012) Multiply twinned Pt-Pd nanoicosahedrons as highly active electrocatalysts for methanol oxidation. Chem Commun 48:543–545
36. Crespo-Quesada M, Andanson JM, Yarulin A, Lim B, Xia Y, Kiwi-Minsker L (2011) UV–ozone cleaning of supported poly (vinylpyrrolidone)-stabilized palladium nanocubes: effect of stabilizer removal on morphology and catalytic behavior. Langmuir 27:7909–7916
37. Xiao L, Zhuang L, Liu Y, Lu J (2008) Activating Pd by morphology tailoring for oxygen reduction. J Am Chem Soc 131:602–608
38. Liang Y, Zhou Y, Ma J, Zhao J, Chen Y, Tang Y, Lu T (2011) Preparation of highly dispersed and ultrafine Pd/C catalyst and its electrocatalytic performance for hydrazine electrooxidation. Appl Catal B Environ 103:388–396
39. Maiyalagan T, Nassr ABA, Alaje TO, Bron M, Scott K (2012) Three-dimensional cubic ordered mesoporous carbon (CMK-8) as highly efficient stable Pd electro-catalyst support for formic acid oxidation. J Power Sources 211:147–153

40. Yang J, Tian C, Wang L, Fu H (2011) An effective strategy for small-sized and highly-dispersed palladium nanoparticles supported on graphene with excellent performance for formic acid oxidation. J Mater Chem A 21:3384–3390

41. Winjobi O, Zhang Z, Liang C, Li W (2010) Carbon nanotube supported platinum–palladium nanoparticles for formic acid oxidation. Electrochim Acta 55:4217–4221